



This is a repository copy of *Switches induced by quorum sensing in a model of enzyme-loaded microparticles*.

White Rose Research Online URL for this paper:
<http://eprints.whiterose.ac.uk/129491/>

Version: Accepted Version

Article:

Bánsági, T. and Taylor, A.F. orcid.org/0000-0003-0071-8306 (2018) Switches induced by quorum sensing in a model of enzyme-loaded microparticles. *Interface*, 15 (140). ISSN 1742-5689

<https://doi.org/10.1098/rsif.2017.0945>

Reuse

Items deposited in White Rose Research Online are protected by copyright, with all rights reserved unless indicated otherwise. They may be downloaded and/or printed for private study, or other acts as permitted by national copyright laws. The publisher or other rights holders may allow further reproduction and re-use of the full text version. This is indicated by the licence information on the White Rose Research Online record for the item.

Takedown

If you consider content in White Rose Research Online to be in breach of UK law, please notify us by emailing eprints@whiterose.ac.uk including the URL of the record and the reason for the withdrawal request.



eprints@whiterose.ac.uk
<https://eprints.whiterose.ac.uk/>

1 Switches Induced by Quorum Sensing in a Model of Enzyme-loaded Microparticles

2 Tamás Bánsági Jr. and Annette F. Taylor

3 Department of Chemical and Biological Engineering, University of Sheffield, S1 3JD, UK

4 **Abstract**

5 Quorum sensing refers to the ability of bacteria and other single-celled organisms to respond to
6 changes in cell density or number with population-wide changes in behaviour. Here, simulations were
7 performed to investigate quorum sensing in groups of diffusively-coupled enzyme microparticles using
8 a well characterised autocatalytic reaction which raises the pH of the medium: hydrolysis of urea by
9 urease. The enzyme urease is found in both plants and microorganisms and has been widely exploited
10 in engineering processes. We demonstrate how increases in group size can be used to achieve a
11 sigmoidal switch in pH at high enzyme loading, oscillations in pH at intermediate enzyme loading and
12 a bistable, hysteretic switch at low enzyme loading. Thus, quorum sensing can be exploited to obtain
13 different types of response in the same system, depending on the enzyme concentration. The
14 implications for microorganisms in colonies are discussed and the results could help in the design of
15 synthetic quorum sensing for biotechnology applications such as drug delivery.

16

17 Keywords: feedback, quorum sensing, enzyme microparticles, switches, oscillations

18

19 **1. Introduction**

20 The remarkable ability of cellular biological systems to coordinate activity has fascinated scientist for
21 decades. The term quorum sensing was first applied to bacteria that displayed a population-wide
22 change in behaviour above a critical density or number of cells, driven by production and release of a
23 small diffusible molecule, the autoinducer, into the environment [1, 2]. In bacteria, increases in cell
24 density can induce bioluminescence and biofilm formation that protects the cells from antibiotics [3].
25 Other micro-organisms such as yeast and the slime mold, *Dictyostelium discoideum*, display density-
26 dependent dynamics including synchronised chemical oscillations above a critical cell density [4, 5].
27 These oscillations play an important part in the life-cycle of *D. discoideum* as they result in travelling
28 waves of cyclic AMP used to direct the motion of cells and formation of multicellular slugs when
29 individual cells are starving [6].

30 More recently quorum sensing has inspired the investigation of synchronous behaviour in
31 various systems including inorganic catalytic micro-particles [7, 8], electronic circuits [9, 10], laser
32 arrays [11] and genetically modified organisms [12]. Although diverse in their underlying mechanisms,
33 common to these systems is some internal means of amplifying a signal (positive feedback) and
34 communication of the signal via a common surround. Combined, these factors drive a sudden sharp
35 change in state across the whole population. Switch-like, ultrasensitive responses can arise in cellular
36 systems through a number of mechanisms; positive feedback is generally required for bistability and
37 oscillations [13]. Applications are beginning to emerge, for example a synthetic quorum sensing circuit
38 in genetically modified bacteria has been exploited for pulsatile drug delivery in vivo [14]. Enzyme-
39 loaded particles or vesicles also have potential applications in medicine [15] and are excellent
40 candidates for synthetic quorum sensing, but evidence of this behaviour has not been reported to
41 date.

42 Mathematical modelling and simulations have provided insight into quorum sensing in both
43 natural and synthetic systems [16-20]. Here, simulations were performed in order to determine the
44 behaviour of groups of enzyme-loaded microparticles in a bath of substrate solution. An enzyme-
45 catalysed reaction was chosen that displays positive feedback through the pH; the urea-urease
46 reaction. This reaction is well characterised and occurs across a variety of plants and cellular organisms

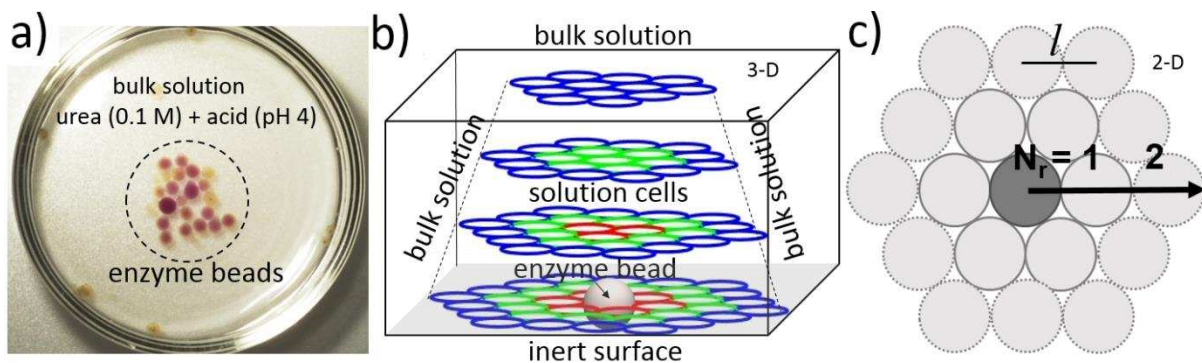
47 [21, 22]. The enzyme urease is a virulence factor produced by certain bacteria and, conversely, has
 48 been used in engineering applications [23], materials synthesis [24, 25] and self-propelled micro- or
 49 nanomotors [26, 27]. Our goal was to determine the types of response that might be obtained with
 50 changes in group size under reaction-diffusion conditions.

51 The model was inspired by ureolytic bacteria such as *Helicobacter pylori* in the acidic, non-
 52 buffered environment of the stomach and *Proteus mirabilis* which colonises the urinary tract and
 53 devices such as catheters [28]. Both of these micro-organisms produce urease to break down urea and
 54 make ammonia thereby raising the pH of their environment. They also form biofilms – communities
 55 of micro-organisms attached to a surface (eg catheter wall) and embedded in glue-like extracellular
 56 polymeric substances (EPS). Small molecules, such as acid and urea, diffuse between the biofilm and
 57 the external solution whereas enzymes are typically confined to the biofilm. Here we used simulations
 58 to determine the collective behaviour of urease-loaded cells under similar conditions.

59 We show that different transitions can be obtained with quorum sensing in the same system.
 60 Three sharp transitions in state, given by the pH, were obtained with increasing the number of
 61 diffusively-coupled urease beads: a sigmoidal switch (a buzzer), oscillations (blinker) and a bistable
 62 switch (toggle) - dynamical responses that all play an important role in the functioning of cells [29, 30].
 63 The generic features are likely to be observed in numerous confined enzyme catalysed reactions that
 64 show feedback. The implications of the results are discussed with regards to cellular organisms, as
 65 well as for applications in biotechnology.
 66

67 2. Model

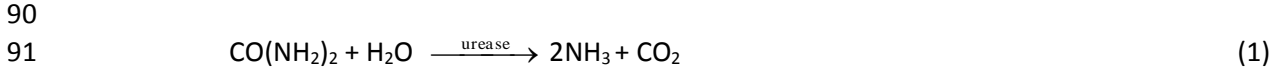
68 The model is designed to mimic experiments [31] in which polymer beads were loaded with the
 69 enzyme urease and placed in a solution of acid (pH 4) and urea in a petri-dish. In earlier work [31, 32]
 70 we explored the behaviour of individual beads. Now we consider the situation, illustrated in Figure 1a,
 71 in which a group of beads are placed in close proximity and loaded with pH indicator to show the
 72 change in pH when the reaction occurs. Complete conversion of urea to ammonia takes several days,
 73 hence the concentrations in the bulk solution are approximately constant over several hours. The
 74 experimental set-up is a grossly simplified version of the biofilm scenario described in the
 75 introduction, however it demonstrates the feasibility of observing the behaviours *in vitro*.
 76



77 Figure 1. (a) Illustration of an experimental set-up with urease-loaded polymer beads placed on the
 78 base of a 5 cm diameter petri-dish containing 50 ml solution of urea (0.1 M) and acid (pH 4). The
 79 enzyme beads contained a pH indicator which is yellow when acidic and purple when basic (pH > 7.5).
 80 (b) The computational domain used in simulations showing in this case a single urease-loaded cell as
 81 a sphere (number of enzyme beads $N_T = 1$) and the surrounding solution cells as circles ($N_S = 94$). The
 82 enzyme bead is directly coupled to the solution cells in red; green cells are next neighbours and blue
 83 cells show 3rd neighbours. The blue solution cells at the edge of the domain are coupled to the bulk
 84 solution with constant concentrations of urea and acid. (c) A 2-D slice of the domain showing a group
 85

86 of hexagonally packed enzyme beads with number of rows $N_r = 2$ and $N_T = 19$. The length scale of cells
 87 in simulations was $l = 100 \mu\text{m}$.

88 The urea-urease reaction results in production of ammonia and an increase in pH through the
 89 following overall processes:



93
 94 Following on from our earlier work, the full model of the reaction was reduced to two variables,
 95 preserving the generic behaviour of the system (see supplementary information for more detail). The
 96 rate of change of substrate concentration, S , and acid concentration, H^+ , was given by:

97
$$\begin{aligned} \frac{dS}{dt} &= D_S \nabla_{\text{hcp}}^2 S - R \\ \frac{d\text{H}^+}{dt} &= \left[D_H \nabla_{\text{hcp}}^2 \left(\text{H}^+ - \frac{K_W}{\text{H}^+} \right) - 2R \right] \left(1 + \frac{K_W}{\text{H}^{+2}} \right)^{-1} \end{aligned} \quad (3)$$

98 where ∇_{hcp}^2 denotes the discrete Laplacian for hexagonal close packing, D_S and D_H are diffusion
 99 constants of substrate urea: $D_S = 1.4 \times 10^{-5} \text{ cm}^2 \text{ s}^{-1}$ and acid: $D_H = 9 \times 10^{-5} \text{ cm}^2 \text{ s}^{-1}$, K_W is the water ion
 100 product from the equilibrium:



103 and R is the rate of the enzyme catalysed step:

104
$$R = \frac{V_{\text{max}} S}{(K_M + S) \left(1 + \frac{K_{\text{es}2}}{\text{H}^+} + \frac{\text{H}^+}{K_{\text{es}1}} \right)} \quad (5)$$

105 This is a modified Michaelis-Menten expression [33, 34] that takes into account the bell-shaped
 106 enzyme rate dependence on acid concentration where $K_{\text{ES}1}$ and $K_{\text{ES}2}$ are the binding constants of the
 107 enzyme to acid: $K_{\text{ES}1} = 5 \times 10^{-6} \text{ M}$, $K_{\text{ES}2} = 2 \times 10^{-9} \text{ M}$. The maximum enzyme rate V_{max} was given by $V_{\text{max}} =$
 108 $k_e E$ where $k_e = 3.7 \times 10^{-6} \text{ M s}^{-1} \text{ u}^{-1} \text{ ml}$ and $E = [\text{enzyme}]$ in u/ml : the enzyme concentration was in
 109 units/ml (M/min/ml) in order to compare with experimental data for urease [22]; and the Michaelis
 110 constant was $K_m = 3 \times 10^{-3} \text{ M}$.

111 Reaction-diffusion simulations were performed on a 3-D hexagonal close packed (hcp) coarse
 112 grid of spatial step size $l = 100 \mu\text{m}$. The hexagonal packing and length scale were chosen to be
 113 amenable to future experimental investigations involving ~ 100 micron-sized enzyme-loaded beads
 114 submerged in a solution of acid and urea. The coarse grid approach allowed us to obtain data from
 115 multiple runs in order to map out behaviour in phase space with both homogeneous and
 116 heterogeneous distributions in enzyme loading. It also allowed us to simulate over a thousand
 117 enzyme-loaded beads with a total length scale $> 1 \text{ cm}$ on a reasonable timescale. A similar approach
 118 has been taken for modelling heterogeneous biofilms in 3-D [35].

119 The computational domain consisted of two types of cell - enzyme-loaded cells (domain Ω_E)
 120 on an inert surface (i.e. the base of the petri-dish) and solution cells (domain Ω_S) containing urea and
 121 acid but no enzyme to represent a thin solution layer at the interface of enzyme loaded beads and the
 122 bulk solution (Figure 1b). The total number of cells in a given simulation was given by the sum of the
 123 enzyme cells and the neighbouring solution cells. Urea and acid diffuse in from the bulk solution
 124 through domain Ω_S and are consumed in the beads resulting in a gradient of these species. We found

125 that with at least three neighbours of solution cells around the enzyme beads the concentrations of
126 acid and substrate approached the constant, bulk solution values smoothly.

127 The total number of enzyme beads was given by $N_T = 3N_r(N_r + 1) + 1$ where N_r indicated the
128 number of rows of enzyme cells after the central cell; an example with $N_r = 2$ is shown in Figure 1c.
129 Changes in group size were achieved by increasing the number of rows of beads. The initial conditions
130 for enzyme beads (domain Ω_E) at $t = 0$ were given by:

$$131 \\ 132 S|_{\Omega_E} = 0 \text{ M and } H^+|_{\Omega_E} = 1 \times 10^{-7} \text{ M with } E = E_0$$

133
134 The solution cells contained no enzyme thus $R = 0$. The initial conditions for solution cells
135 (domain Ω_S) at $t = 0$ were given by:

$$136 \\ 137 S|_{\Omega_S} = S_0 \text{ and } H^+|_{\Omega_S} = H_0 \text{ with } E = 0$$

138
139 where S_0 and H_0 are the bulk solution concentrations. The value of H_0 in all simulations was $1 \times 10^{-4} \text{ M}$
140 ($\text{pH}_0 = 4$) whilst S_0 and E_0 were varied.

141 A Dirichlet boundary condition was applied at the sides and top of the solution cells (boundary
142 $\partial\Omega_s$) to provide the cells with a constant supply of substrate and acid from the bulk solution (i.e. the
143 solution in the rest of the petri-dish):

$$144 \\ 145 S|_{\partial\Omega_s} = S_0 \text{ and } H^+|_{\partial\Omega_s} = H_0$$

146
147 No-flux Neuman boundary conditions were applied at the base of the domain (boundary $\partial\Omega_b$) to
148 simulate the diffusion barrier at the base of the petri-dish:

$$149 \\ 150 \nabla S|_{\partial\Omega_b} = 0 \text{ and } \nabla H^+|_{\partial\Omega_b} = 0$$

151
152 For heterogeneous loadings, simulations were performed using a normal (Gaussian) random number
153 generator for enzyme concentration, with mean μ_E and coefficient of variation $\sigma = 10 - 30\%$. Data from
154 eleven runs with different initial spatial distributions of enzyme was collected for each value of μ_E and
155 σ and the number of times a resultant behaviour (high pH steady state, oscillatory, low pH steady
156 state) occurred was recorded relative to the total number of runs.

157

158 **3. Results**

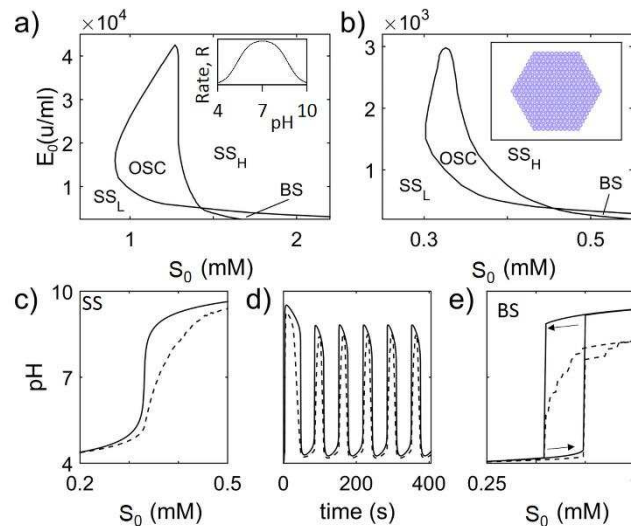
159 **3.1 Switches with substrate**

160
161 The behaviour of a single enzyme bead in substrate solution was mapped out in enzyme-
162 substrate space (Fig. 2a). Positive feedback in the urea-urease reaction is driven by the product,
163 ammonia, and the bell-shaped rate-pH curve (inset, Fig. 2a). The maximum enzyme rate is at pH 7,
164 correlated with a maximum in the active form of the enzyme. If the enzyme is in a solution of acid, the
165 rate is initially low. The production of ammonia raises the pH and rate of reaction accelerates. Negative
166 feedback was provided by the constant supply of acid by diffusion from the surrounding solution [32].

167 Although ammonia was not explicitly included in the two-variable model, its concentration is
168 correlated with the pH. A cross-shaped phase diagram was obtained, where at low substrate, S_0 , and
169 enzyme concentration, E_0 , the ammonia was produced at an insufficient rate compared to the influx
170 of acid from the surround resulting in an unreacted, low pH steady state (SS_L) in the bead. At high S_0
171 and E_0 the rate of reaction is high enough to overcome the influx of acid and the bead switched to a
172 reacted, high pH state (SS_H). Separating these two states are regions of oscillations (OSC) or bistability

173 (BS) in pH. The results qualitatively agree with previous findings obtained in 2- and 8-variable
 174 compartment models of the urea-urease reaction [32].

175 The phase diagram for a hexagonal array of beads with number of rows $N_r = 10$ is shown in
 176 Figure 2b. Increasing the number of beads shifted the high pH states to lower enzyme and substrate
 177 concentrations, but the same general features were preserved. Three different types of transition
 178 were obtained with increasing substrate: a sigmoidal switch in pH at high enzyme (Fig. 2c), switch to
 179 oscillations at intermediate enzyme (Fig. 2d) and a bistable switch at low enzyme concentrations (Fig.
 180 2e). The beads at the edge of the group typically had a lower pH than the central beads resulting in a
 181 reduced average pH over the entire domain (dotted line). These transitions may be considered
 182 switches in the sense that there is a sharp change from an “off” (low pH) state to an “on” (high pH)
 183 state.



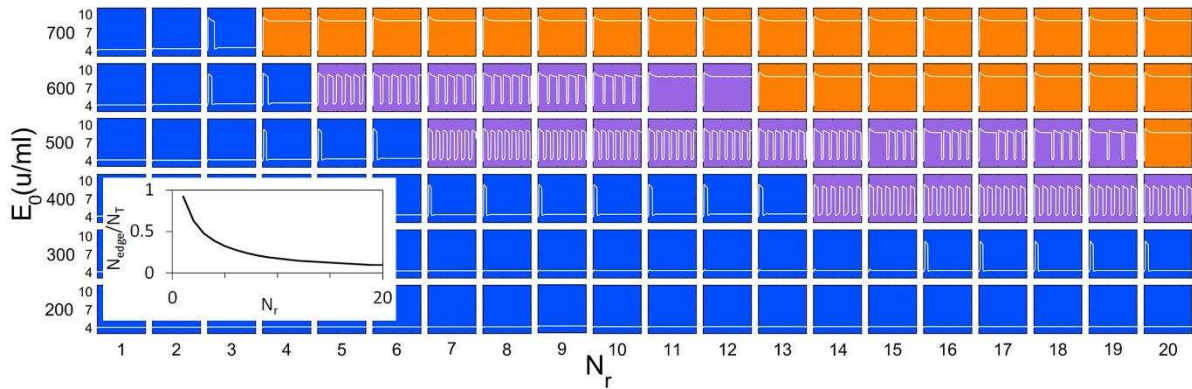
184 Figure 2. Phase diagram as a function of enzyme and substrate concentrations mapping dynamic
 185 behaviour of (a) single 100 μm bead and (b) group of 100 μm beads with $N_r = 10$ and low pH state
 186 (SS_L), high pH state (SS_H), bistable (BS) and oscillatory (OSC). With $N_r = 6$: (c) sigmoidal switch in pH
 187 with $E_0 = 8000$ u/ml; (d) oscillations in time with $E_0 = 1000$ u/ml; (e) bistable switch with $E_0 = 200$ u/ml.
 188 In (c – e) central bead pH (thick line) and average pH of the group (dotted line).
 189

190
 191

192 **3.2 Switches with group size**

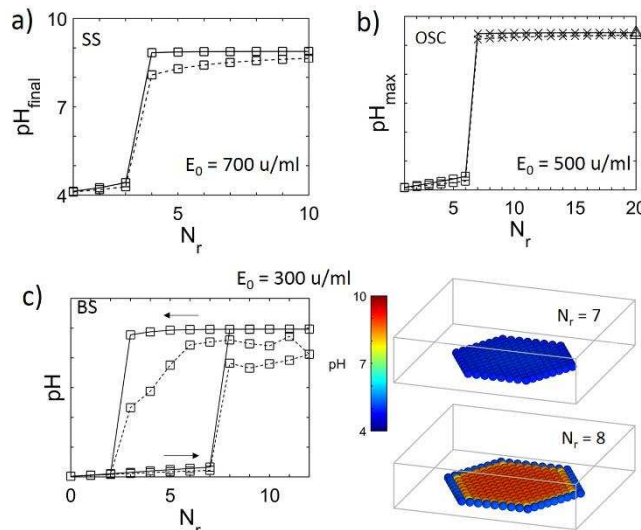
193

194 The same three types of transition were obtained if instead of increasing substrate, the concentration
 195 of substrate was fixed and the number of rows of beads (N_r) was increased. An E_0 - N_r phase diagram is
 196 plotted in Figure 3 showing regions of low pH steady state (blue, SS_L), oscillations (purple, OSC) and
 197 high pH steady state (orange, SS_H). Increasing N_r had a similar effect to increasing substrate. When the
 198 N_r is < 4 , acid diffused in from the surround keeping the concentration of ammonia and the pH low in
 199 the beads. The inset shows the number of beads at the edges or the array compared to total number
 200 of beads ($N_{\text{edge}}/N_T = 3/(3(N_r+1)+1/N_r)$). As N_r was increased, a smaller fraction of the beads was in
 201 contact with the acid at the edges of the array and a sharp transition to a high pH state or oscillations
 202 was obtained.
 203



204 Figure 3. Phase diagram as a function of enzyme concentration and number of rows of enzyme beads
 205 where blue = SS_L , purple = OSC and orange = SS_H . The tiles show the pH in time of the central bead and
 206 the inset shows the ratio of edge beads to total beads with increasing N_r . The value of $S_0 = 0.4$ mM.
 207
 208

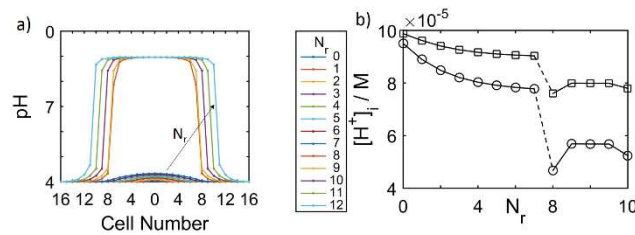
209 With $S_0 = 0.4$ mM and $E_0 = 600$ u/ml, a switch from low to high pH was obtained (Fig. 4a). When
 210 E_0 was decreased, oscillations were observed above a threshold number of cells (Fig. 4b). A bistable
 211 switch could not be obtained with reasonable values of N_r with $S_0 = 0.4$ mM; the fraction of edge beads
 212 approached zero with $N_r = 20$, thus little change was observed in the dynamics for larger number of
 213 rows. However, bistability was obtained within the range $N_r = 1 - 20$ when $S = 0.5$ mM, as shown in
 214 Figure 4c.



215 Figure 4. Switches in pH with number of rows of beads. (a) Sigmoidal switch, (b) switch to oscillations
 216 (maximum pH shown), (c) bistable switch and pH of beads in the array with $N_r = 7$ (SS_L) and 8 (SS_H).
 217 The central bead pH (thick line) and average pH of the group (dotted line) are shown and $S_0 = 0.4$ mM
 218 in (a – b) and $S_0 = 0.5$ mM in (c).
 219
 220

221 Quorum sensing is typically associated with increases in the autoinducer concentration in
 222 solution and/or the rate of loss of autoinducer initiating autocatalysis as the number of cells is
 223 increased (one does not necessarily imply the other) [8]. Here, the transition was correlated with the
 224 change in pH and hence acid concentration. The pH profile across a central slice of the array is shown
 225 in Figure 5a for the same conditions as in Figure 4c. For $N_r < 8$, the pH across the group was low (< 5),
 226 and a gradient in pH can be seen from the centre bead outwards. The pH was lowest at the edges of
 227 the group where the beads were in contact with the acid solution from both the side and above. As N_r
 228 was increased, the pH of all the beads increased as a result of the decrease in the fraction of edge
 229 beads. At $N_r = 8$ there was a large amplitude increase in pH across the group. Correspondingly, the acid
 230 concentration fell to a threshold level in both the edge beads and the adjacent solution cells up to N_r

231 = 7 (Fig. 5b). Note however the difference between the edge beads and solution acid concentration
 232 increased. So the increased reaction rate with increasing pH must overcome the increased influx rate
 233 of acid to initiate autocatalysis.
 234



235 Figure 5. Switch in pH with increasing number of rows from 1 – 12 for conditions in Figure 4c. (a) pH
 236 profiles and (b) Concentration of acid in beads at the edge of the group (lower curve, circles) and
 237 adjacent solution cells (upper curve, squares). Dashed lines indicate the transition to the high pH state.
 238
 239

240 With the substrate and acid concentrations fixed, the critical N_r for a change in state and the outcome
 241 of the transition, whether to oscillations or high pH steady state, was determined by the enzyme
 242 concentration. The threshold increased with decreasing E_0 (Fig. 3).
 243

244 3.2.1 Sigmoidal switch with N_r

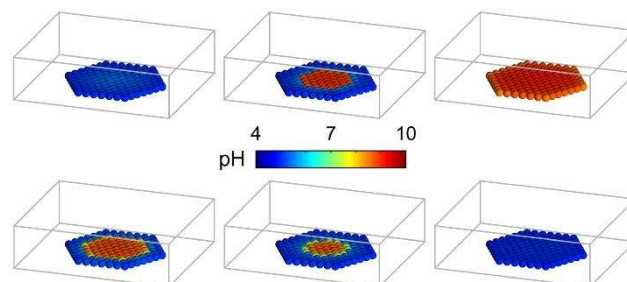
245 A sigmoidal switch in pH was obtained for sufficiently high enzyme ($E_0 > 600$ u/ml in Fig. 3)
 246 with increasing the number of rows of beads. Sigmoidal switches are reversible: in Figure 4a a large
 247 amplitude increase in pH occurred as N_r was increased from 3 to 4 and decreasing N_r back to 3 resulted
 248 in a drop back to low pH. This switch is referred to as a buzzer [29] because the “on” state is reached
 249 whenever a parameter, here N_r , is raised above a single threshold value.
 250

251 3.2.2 Bistable switch with N_r

252 Bistable switches in pH were obtained with a low concentration of enzyme ($E_0 = 300$ u/ml in
 253 Fig. 4c). The value of the pH was dependent on the system history. So if N_r was increased, the beads
 254 remained in a low pH state until a threshold was reached at $N_r = 8$ then the pH switched to high. If N_r
 255 was then decreased, the pH remained in a high state until the lower limit of $N_r = 3$ when it dropped
 256 back down. Between these values the low and high pH state coexisted. This is an example of a toggle
 257 switch [29] in the sense that it can be flipped between the “on” (high pH) and “off” (low pH) states.
 258

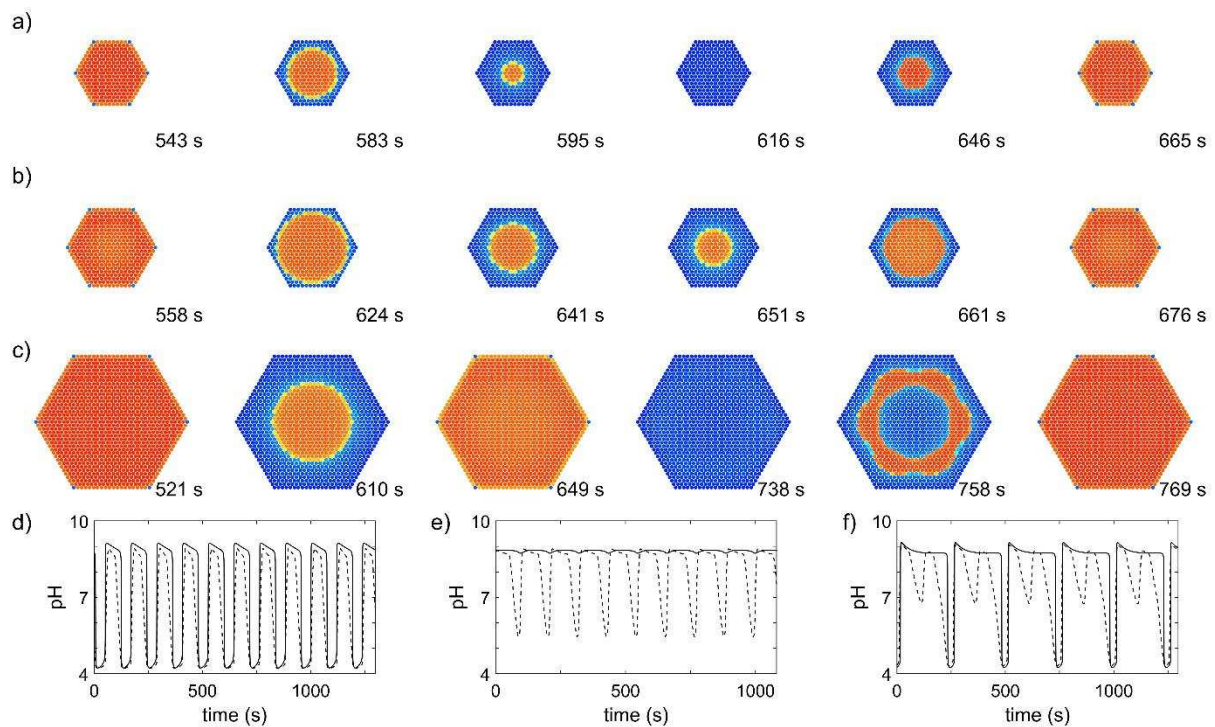
259 3.2.3 Oscillations with N_r

260 A transition to oscillatory behaviour occurred at intermediate enzyme levels ($E_0 = 400 - 600$
 261 u/ml in Fig. 3). A time series of the oscillatory state, referred to as a blinker [29], is shown in Figure 6.
 262 The array did not oscillate uniformly; there was a phase lag between the centre and the outer edge of
 263 the array.
 264



265 Figure 6. Illustration of oscillatory behaviour in an array of urease beads with $S_0 = 0.4$ mM, $E_0 = 600$
 266 u/ml and the number of rows of beads $N_r = 6$ (surrounding solution cells not shown). Movie available
 267 at [link](#).
 268
 269

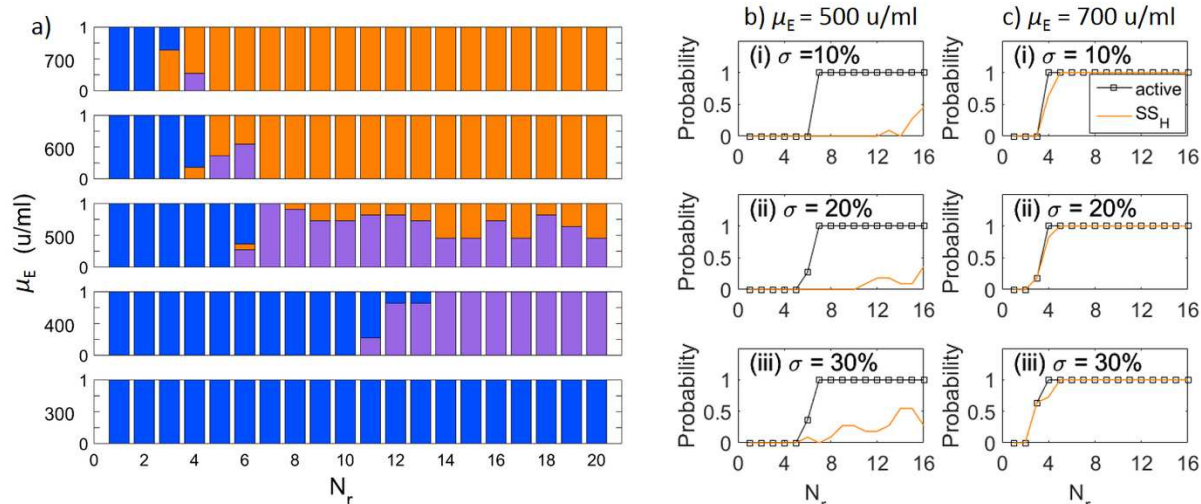
270 Different types of oscillatory dynamics were observed depending on the size of the group and
 271 enzyme concentrations. For $N_r = 9$, and $E_0 = 500$ u/ml the whole group oscillated with a front spreading
 272 from the centre of the array outwards and then contracting in from the edges (Fig. 7a). The length
 273 scale of the array ($23 \times 100 \mu\text{m} = 2.3$ mm) was small and a reaction-diffusion wave was not observed;
 274 the acid diffused in from the edge quenching the high pH state before recovery of the central beads
 275 could take place. For larger enzyme, $E_0 = 600$ u/ml, and $N_r = 11$ the central cells remained in the high
 276 pH state while the outer cells oscillated (Fig. 7b). This is a mixed high pH-blinker state. A dual frequency
 277 state was also observed as the number of rows was increased to $N_r = 19$, where the edge beads
 278 oscillated with double the frequency of the centre beads (Fig. 7c).
 279



280
 281 Figure 7. Oscillatory dynamics of bead arrays with $S_0 = 0.4$ mM and pH time traces show central bead
 282 pH (thick line) and average pH of array (dotted line). (a) and (d) Blinker with $E_0 = 500$ u/ml and $N_r = 9$;
 283 (b) and (e) mixed high pH-blinker state with $E = 600$ u/ml and $N_r = 11$; (c) and (f) dual frequency state
 284 $E_0 = 500$ u/ml and $N_r = 19$. Movies available at a) [link](#), b) [link](#) and c) [link](#).
 285
 286

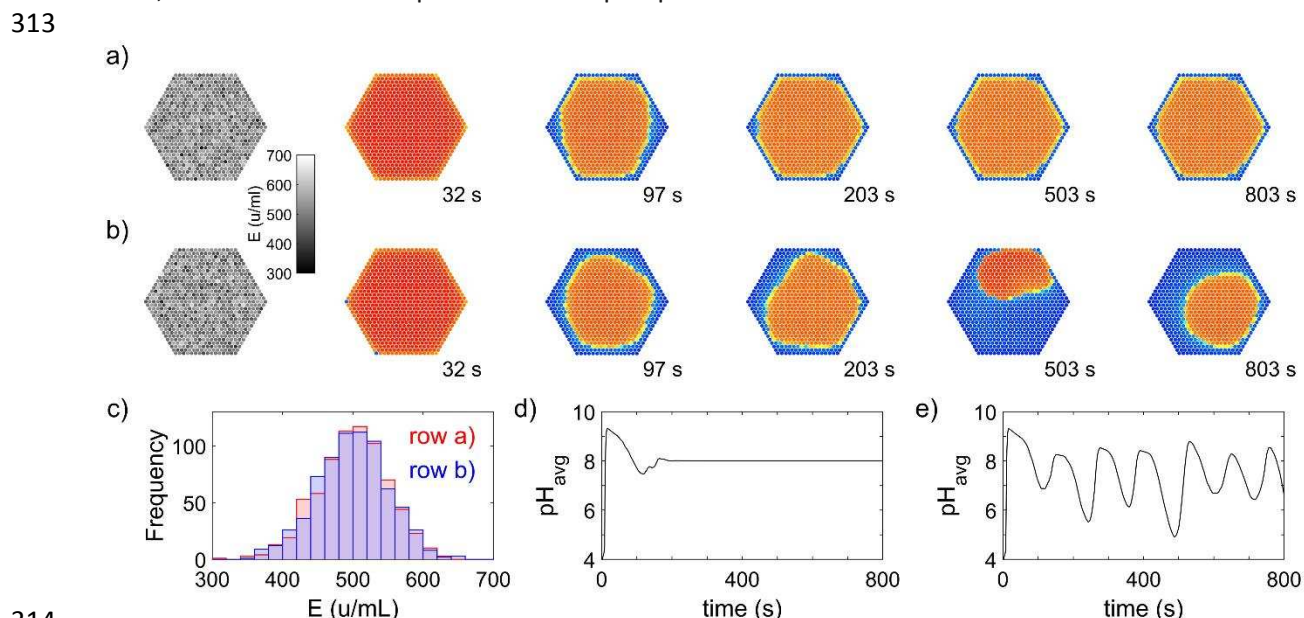
287 **3.3 Transitions with numbers of beads: heterogeneous distributions of enzyme**

288
 289 The influence of heterogeneity in enzyme loading on these dynamical transitions was also
 290 investigated with values of E selected randomly from a normal distribution. Multiple runs were
 291 performed to estimate the probability of a high pH steady state (SS_H), oscillatory (OSC) or low pH
 292 steady state (SS_L) for a given mean enzyme activity μ_E and coefficient of variation, σ . The resulting μ_E -
 293 N_r phase diagram was similar in form to Figure 3, even with $\sigma = 30\%$ (Fig. 8a). The sharp transitions
 294 with N_r were still obtained, resulting in a sigmoidal switch at $\mu_E = 700$ u/ml and a transition to
 295 oscillations at $\mu_E = 500$ u/ml (Figure 8b, c). However, with $\mu_E = 500$ u/ml, there was an increased
 296 probability of the high pH steady state as N_r and σ were increased.
 297



298
 299 Figure 8. Switches in heterogeneous enzyme arrays with $S_0 = 0.4$ mM, $pH_0 = 4$ and $\mu_E =$ mean enzyme
 300 activity. (a) Phase diagram with $\sigma = 30\%$ where each bar shows fraction of SS_H (orange), SS_L (blue) or
 301 OSC (purple) obtained from multiple runs. (b) and (c) Probability of either SS_H or OSC (active, black
 302 squares) and probability of SS_H (orange line) with (b) $E = 500$ u/ml and (c) $E = 700$ u/ml.

303
 304 The spatial distribution of the enzyme played an important role in the selection of dynamical
 305 behaviour; SS_H or OSC. In two separate runs with $\mu_E = 500$ u/ml and $\sigma = 10\%$, an oscillatory state was
 306 obtained with total enzyme of $E_T = 3.6162 \times 10^5$ u/ml and a high pH steady state was obtained with
 307 lower total enzyme $E_T = 3.6004 \times 10^5$ u/ml. The formation of the steady state and an oscillatory state
 308 are shown in Figure 9, as well as the spatial configuration of the enzyme concentration (greyscale) and
 309 normal distribution of enzyme (Fig. 9c). Waves propagated asymmetrically across the domain in case
 310 b, resulting in travelling structures that gave rise to aperiodic average pH-time traces. The time-
 311 average pH over the array was 8 in the case of the steady state and less than that in the oscillatory
 312 case; however individual spikes reached up to pH 9.



314
 315 Figure 9. Dynamic behaviour in heterogeneous enzyme arrays with $\mu_E = 500$ u/ml, $\sigma = 10\%$ and $S_0 = 0.4$
 316 mM and $N_r = 15$. First image shows spatial enzyme distribution and subsequent evolution of the array
 317 is shown in a series of images where blue = low pH, orange = high pH. (a) Steady state and (b)
 318 oscillations. (c) Normal distribution of enzyme loading; (d) and (e) average pH in the array in time for
 319 (a) and (b) respectively. Movie for (b) available at [link](#).

321

322 4. Discussion

323 Here we examined transitions in the behaviour of groups of enzyme-loaded microparticles
324 (beads) that displayed feedback and exchanged chemicals with a common surround via passive
325 diffusion. Our coarse grid approach with the two-variable model allowed us to explore parameter
326 space and identify some generic features that may aid in the implementation of synthetic quorum
327 sensing in applications. The simulations were inspired by quorum sensing in bacteria and other single
328 celled organisms and, although clearly an oversimplification, may provide some insight to some of the
329 dynamic behaviours observed in growing colonies of microorganisms.

330 The term quorum sensing refers to a population-wide change in behaviour above a threshold
331 number or density of cells [1, 3]. In line with other work, we considered quorum sensing transitions in
332 a uniform layer of cells with constant local density but growing in size [16]. However, the spatial
333 proximity of cells within a colony may play a role in such transitions, as well as other processes that
334 influence the mass transfer such as advection. This has led to the introduction of the terms “diffusion
335 sensing” and later “efficiency sensing” in order to take into account these factors [36]. Simulations
336 were performed with heterogeneities in enzyme loading which likely play a similar role to clustering
337 effects although this warrants further investigation. Nevertheless, we found that the sharp changes in
338 state with increasing group size were robust.

339 Quorum sensing in cells involves the production and release of small diffusible molecules into
340 the extracellular solution. Changes in state are generally associated with a build-up of autoinducer in
341 the surrounding solution to some threshold level or a decrease in the loss rate of autoinducer from
342 cells by diffusion [8, 16]. One or more autoinducers may be involved in a complex network of reactions.
343 For example, *Dictyostelium* cells use the molecules PSF and cAMP as intercellular signals [37]. PSF
344 accumulates in the extracellular solution with increasing cell density. When PSF reaches a threshold
345 level and food is in short supply, this glycoprotein initiates a series of processes resulting in activation
346 of the enzyme required for cAMP synthesis. The cAMP catalyses its own production and is emitted in
347 pulses, propagating as waves through the colony that direct the motion of cells.

348 Here, a well characterised enzyme-catalysed reaction was selected that is both present in
349 microorganisms and accessible in vitro: the urea-urease reaction [22]. In a simple analogy to a
350 biological quorum sensing circuit, the enzyme, urease, was confined to a microparticle and cell-to-cell
351 communication was achieved through diffusion of acid and substrate. The enzyme reaction raised the
352 pH and feedback occurred as an increase in pH led to an increase in rate. An individual bead was
353 unable to raise the pH sufficiently to overcome the influx of acid from the surrounding solution.
354 However, in a group of beads there was a lower fraction of beads in contact with acid at the edge of
355 the array and the pH increased in both the beads and the adjacent solution cells to some threshold
356 level, initiating autocatalysis.

357 The signal-response curves obtained here are switch-like in the sense that there is a change
358 from a low pH “off” state to a high pH “on” state with increases in group size. The nature of the switch
359 was found to depend upon the enzyme concentration of the beads: at high enzyme a sigmoidal switch
360 (buzzer) was obtained; at intermediate enzyme oscillations were observed (blinker) and at low enzyme
361 a bistable (toggle) switch resulted. These are all important dynamical responses that arise in cellular
362 systems [29] and the results have some interesting implications for growing colonies of micro-
363 organisms.

364 If cells contain sufficient enzyme, then a sharp transition to a high autoinducer “on” state is
365 obtained with increasing group size. This switch, the buzzer, is not robust as small changes in
366 parameters in the vicinity of the transition point result in collapse of the behaviour, however the cells
367 are producing large amounts of enzyme. If the cells contain intermediate amounts of enzyme, an
368 increase in the group size results in an oscillating state, a blinker. The amount of autoinducer produced
369 in time is lower than for the sigmoidal switch, but conversion is still achieved, and pulses of
370 autoinducer can be used to direct the motion of cells.

371 For low enzyme concentrations, the system displays a bistable toggle switch with increasing
372 group size. This is useful, since the cells are producing small amounts of enzyme but the switch is
373 robust to noise under these conditions. Once the transition to the “on” state is made, small changes
374 in group size or substrate concentration do not lead to a return to the low autoinducer state.

375 Although it is not implicated in quorum sensing, the enzyme urease is a virulence factor
376 exploited by bacteria such as *Helicobacter pylori* and *Proteus mirabilis* in the non-buffered
377 environment of the stomach or urinary tract. The increase in pH associated with the reaction is
378 believed to protect *H. pylori* against the acidic environment of stomach [38]. *P. mirabilis* forms rafts –
379 small groups of cells linked together - that allow the bacteria to rapidly colonise catheters. Cells
380 produce a particularly potent urease that drives an increase of urine pH and precipitation of
381 phosphates leading to the formation of kidney stones and catheter encrustations [28]. We have shown
382 how sharp switches in pH can be obtained when a group reaches a critical size. There may be gradients
383 in pH in time and space but with feedback the maximum pH obtained locally can result in sufficiently
384 high values to trigger rapid biomineralisation, even if the average pH of the whole system is lower. It
385 would be of interest to couple the enzyme processes included here with cell motion in order to better
386 understand how feedback through pH may influence pathogenic behaviour [39].

387 The main reason for our choice of urease was that the system reported here is implementable
388 in experiments. Urease has been used in sensing, crack repair (by inducing calcium carbonate
389 precipitation) [40] and polymer synthesis [24] and has been immobilised on numerous solid supports
390 including alginate [41]. In earlier work, it was demonstrated how features such as waves and
391 oscillations obtained in the two-variable urea-urease model are also possible in the full model
392 including all chemical processes and enzyme inhibition, albeit over a smaller region of parameter
393 space [32, 42]. Propagating waves of pH and bistable switches have been obtained in the gel beads,
394 but oscillations were not observed, probably because a key requirement is the differential transport
395 ($D_H > D_S$) of acid and substrate, and diffusion constants for acid in gels may be lower than for dilute
396 solutions [43]. Evidence of collective behaviour has not yet been reported in urease beads.

397 The cross-shaped phase diagram is a universal map, spanning many different mechanisms of
398 autocatalysis, that has been used to find oscillations and patterns in chemical systems [44]. The same
399 general topology was obtained here in enzyme-substrate and enzyme-group size phase space. The
400 feedback mechanism exploited involves coupling the bell-shaped rate–pH curve with production of an
401 acid or base. Originally proposed in simulations with an esterase [45], this method is widely applicable
402 since most enzymes display similar rate–pH curves [46]. It seems likely that a similar diagram will be
403 obtained for other enzyme-catalysed reactions, as well as other autocatalytic processes.

404 Synthetic quorum sensing might be exploited in biotechnology to induce a sharp change in
405 state in response to a change in a density- or group size in, for example, targeted drug delivery.
406 Collective behaviour has been extensively investigated in inorganic catalytic particles and more
407 complex behaviours than reported here are possible [47, 48]. However, for applications in medicine
408 biocompatible feedback is required. Feedback itself is widely used for complex information processing
409 in biological cells. There is increasing interest in the design of bio-compatible reaction networks
410 involving organic molecules [49, 50], peptides, enzymes [51, 52] and even DNA [53, 54] that might be
411 used to generate bio-inspired emergent behaviour in synthetic systems [55]. Enzyme-loaded
412 microparticles or vesicles remain the best candidates for obtaining collective behaviour inspired by
413 bacteria such as quorum sensing.

414

415 5. Conclusions

416 We have demonstrated in reaction-diffusion simulations how three different transitions can
417 be achieved with increasing numbers of enzyme-loaded microparticles: a sigmoidal buzzer, an
418 oscillatory blinker and bistable toggle switch. The simulations exploited the use of a single enzyme,
419 urease, found in numerous plants and microorganisms, that raises the pH of the medium and
420 experimental implementation of the results is feasible. The combination of cell-to-cell communication

421 and feedback might be exploited to generate more complex collective behaviours and spatial
422 organisation in enzyme catalytic particles for bioinspired dynamic materials or devices.

423

424 [Data accessibility](#)

425 Supplementary information, movies and code are available at the University of Sheffield repository
426 ORDA: 10.15131/shef.data.5357494; 10.15131/shef.data.5357503 and 10.15131/shef.data.5357506.

427 [Authors' contributions](#)

428 TB and AFT conceived the study, TB wrote the code and collected the data, AFT and TB performed
429 data analysis and wrote the manuscript.

430 [Competing interests](#)

431 We declare that we have no competing interests.

432 [Funding](#)

433 The research was supported by Engineering and Physical Science Research Council grant
434 EP/K030574/2.

435

436 **References**

- 437 [1] Waters, C.M. & Bassler, B.L. 2005 Quorum sensing: Cell-to-cell communication in bacteria. In
438 *Annu. Rev. Cell Dev. Biol.* (pp. 319-346).
- 439 [2] Fuqua, W.C., Winans, S.C. & Greenberg, E.P. 1994 Quorum sensing in bacteria: The LuxR-LuxI
440 family of cell density- responsive transcriptional regulators. *J. Bacteriol.* **176**, 269-275.
- 441 [3] Davies, D.G., Parsek, M.R., Pearson, J.P., Iglewski, B.H., Costerton, J.W. & Greenberg, E.P. 1998
442 The involvement of cell-to-cell signals in the development of a bacterial biofilm. *Science* **280**, 295-
443 298. (doi:10.1126/science.280.5361.295).
- 444 [4] De Monte, S., D'Ovidio, F., Danø, S. & Sørensen, P.G. 2007 Dynamical quorum sensing: Population
445 density encoded in cellular dynamics. *Proc. Natl. Acad. Sci. U.S.A.* **104**, 18377-18381.
446 (doi:10.1073/pnas.0706089104).
- 447 [5] Nanjundiah, V. 1998 Cyclic AMP oscillations in dictyostelium discoideum: Models and
448 observations. *Biophys. Chem.* **72**, 1-8. (doi:10.1016/S0301-4622(98)00118-5).
- 449 [6] Du, Q., Kawabe, Y., Schilde, C., Chen, Z.H. & Schaap, P. 2015 The Evolution of Aggregative
450 Multicellularity and Cell-Cell Communication in the Dictyostelia. *J. Mol. Biol.* **427**, 3722-3733.
451 (doi:10.1016/j.jmb.2015.08.008).
- 452 [7] Taylor, A.F., Tinsley, M.R., Wang, F., Huang, Z. & Showalter, K. 2009 Dynamical quorum sensing
453 and synchronization in large populations of chemical oscillators. *Science* **323**, 614-617.
454 (doi:10.1126/science.1166253).
- 455 [8] Tinsley, M.R., Taylor, A.F., Huang, Z. & Showalter, K. 2009 Emergence of collective behavior in
456 groups of excitable catalyst-loaded particles: Spatiotemporal dynamical quorum sensing. *Phys. Rev.*
457 *Lett.* **102**. (doi:10.1103/PhysRevLett.102.158301).
- 458 [9] Singh, H. & Parmananda, P. 2013 Quorum sensing via static coupling demonstrated by Chua's
459 circuits. *Physical Review E - Statistical, Nonlinear, and Soft Matter Physics* **88**.
460 (doi:10.1103/PhysRevE.88.040903).
- 461 [10] Hellen, E.H., Dana, S.K., Zhurov, B. & Volkov, E. 2013 Electronic Implementation of a
462 Repressilator with Quorum Sensing Feedback. *PLoS ONE* **8**. (doi:10.1371/journal.pone.0062997).
- 463 [11] Zamora-Munt, J., Masoller, C., Garcia-Ojalvo, J. & Roy, R. 2010 Crowd synchrony and quorum
464 sensing in delay-coupled lasers. *Phys. Rev. Lett.* **105**. (doi:10.1103/PhysRevLett.105.264101).

465 [12] Danino, T., Mondragón-Palomino, O., Tsimring, L. & Hasty, J. 2010 A synchronized quorum of
466 genetic clocks. *Nature* **463**, 326-330. (doi:10.1038/nature08753).

467 [13] Ferrell, J.E., Jr. & Ha, S.H. 2014 Ultrasensitivity part III: Cascades, bistable switches, and
468 oscillators. *Trends Biochem. Sci* **39**, 612-618. (doi:10.1016/j.tibs.2014.10.002).

469 [14] Din, M.O., Danino, T., Prindle, A., Skalak, M., Selimkhanov, J., Allen, K., Julio, E., Atolia, E.,
470 Tsimring, L.S., Bhatia, S.N., et al. 2016 Synchronized cycles of bacterial lysis for in vivo delivery.
471 *Nature* **536**, 81-85. (doi:10.1038/nature18930).

472 [15] Kuchler, A., Yoshimoto, M., Luginbühl, S., Mavelli, F. & Walde, P. 2016 Enzymatic reactions in
473 confined environments. *Nature Nanotechnology* **11**, 409-420. (doi:10.1038/nnano.2016.54).

474 [16] Dockery, J.D. & Keener, J.P. 2001 A mathematical model for quorum sensing in *Pseudomonas*
475 *aeruginosa*. *Bull. Math. Biol.* **63**, 95-116. (doi:10.1006/bulm.2000.0205).

476 [17] Garcia-Ojalvo, J., Elowitz, M.B. & Strogatz, S.H. 2004 Modeling a synthetic multicellular clock:
477 Repressilators coupled by quorum sensing. *Proc. Natl. Acad. Sci. U.S.A.* **101**, 10955-10960.
478 (doi:10.1073/pnas.0307095101).

479 [18] Shum, H. & Balazs, A.C. 2017 Synthetic quorum sensing in model microcapsule colonies. *Proc.*
480 *Natl. Acad. Sci. U.S.A.* **114**, 8475-8480. (doi:10.1073/pnas.1702288114).

481 [19] Gou, J. & Ward, M.J. 2016 An Asymptotic Analysis of a 2-D Model of Dynamically Active
482 Compartments Coupled by Bulk Diffusion. *Journal of Nonlinear Science* **26**, 979-1029.
483 (doi:10.1007/s00332-016-9296-7).

484 [20] Popat, R., Cornforth, D.M., McNally, L. & Brown, S.P. 2015 Collective sensing and collective
485 responses in quorum-sensing bacteria. *Journal of the Royal Society Interface* **12**.
486 (doi:10.1098/rsif.2014.0882).

487 [21] Krajewska, B. 2009 Ureases I. Functional, catalytic and kinetic properties: A review. *J. Mol. Catal.*
488 *B: Enzym.* **59**, 9-21. (doi:10.1016/j.molcatb.2009.01.003).

489 [22] Hu, G., Pojman, J.A., Scott, S.K., Wrobel, M.M. & Taylor, A.F. 2010 Base-catalyzed feedback in
490 the urea-urease reaction. *J. Phys. Chem. B* **114**, 14059-14063. (doi:10.1021/jp106532d).

491 [23] Phillips, A.J., Gerlach, R., Lauchnor, E., Mitchell, A.C., Cunningham, A.B. & Spangler, L. 2013
492 Engineered applications of ureolytic biomineralization: A review. *Biofouling* **29**, 715-733.
493 (doi:10.1080/08927014.2013.796550).

494 [24] Heuser, T., Weyandt, E. & Walther, A. 2015 Biocatalytic Feedback-Driven Temporal
495 Programming of Self-Regulating Peptide Hydrogels. *Angewandte Chemie - International Edition* **54**,
496 13258-13262. (doi:10.1002/anie.201505013).

497 [25] Jee, E., Bánsági, T., Jr., Taylor, A.F. & Pojman, J.A. 2016 Temporal control of gelation and
498 polymerization fronts driven by an autocatalytic enzyme reaction. *Angewandte Chemie -*
499 *International Edition* **55**, 2127-2131. (doi:10.1002/anie.201510604).

500 [26] Ma, X., Jannasch, A., Albrecht, U.R., Hahn, K., Miguel-López, A., Schäffer, E. & Sánchez, S. 2015
501 Enzyme-Powered Hollow Mesoporous Janus Nanomotors. *Nano Lett.* **15**, 7043-7050.
502 (doi:10.1021/acs.nanolett.5b03100).

503 [27] Dey, K.K., Zhao, X., Tansi, B.M., Méndez-Ortiz, W.J., Córdova-Figueroa, U.M., Golestanian, R. &
504 Sen, A. 2015 Micromotors Powered by Enzyme Catalysis. *Nano Lett.* **15**, 8311-8315.
505 (doi:10.1021/acs.nanolett.5b03935).

506 [28] Stickler, D.J. 2008 Bacterial biofilms in patients with indwelling urinary catheters. *Nat. Clin.*
507 *Pract. Urol.* **5**, 598-608. (doi:10.1038/ncpuro1231).

508 [29] Tyson, J.J., Chen, K.C. & Novak, B. 2003 Sniffers, buzzers, toggles and blinkers: Dynamics of
509 regulatory and signaling pathways in the cell. *Curr. Opin. Cell Biol.* **15**, 221-231. (doi:10.1016/S0955-
510 0674(03)00017-6).

511 [30] Tyson, J.J., Albert, R., Goldbeter, A., Ruoff, P. & Sible, J. 2008 Biological switches and clocks.
512 *Journal of the Royal Society Interface* **5**, S1-S8. (doi:10.1098/rsif.2008.0179.focus).

513 [31] Muzika, F., Bansagi, T., Jr., Schreiber, I., Schreiberova, L. & Taylor, A.F. 2014 A bistable switch in
514 pH in urease-loaded alginate beads. *Chem Commun (Camb)* **50**, 11107-11109.
515 (doi:10.1039/c4cc03936j).

516 [32] Bánsági, T. & Taylor, A.F. 2014 Role of differential transport in an oscillatory enzyme reaction. *J.*
517 *Phys. Chem. B* **118**, 6092-6097. (doi:10.1021/jp5019795).

518 [33] Chang, R. 2005 Enzyme kinetics. In *Physical Chemistry for the Biosciences* (University Science
519 Books).

520 [34] Krajewska, B. & Ciurli, S. 2005 Jack bean (*Canavalia ensiformis*) urease. Probing acid-base groups
521 of the active site by pH variation. *Plant Physiology and Biochemistry* **43**, 651-658.
522 (doi:10.1016/j.plaphy.2005.05.009).

523 [35] Picioareanu, C., Kreft, J.U. & Van Loosdrecht, M.C.M. 2004 Particle-based multidimensional
524 multispecies biofilm model. *Applied and Environmental Microbiology* **70**, 3024-3040.
525 (doi:10.1128/AEM.70.5.3024-3040.2004).

526 [36] Hense, B.A., Kuttler, C., Müller, J., Rothballer, M., Hartmann, A. & Kreft, J.U. 2007 Does
527 efficiency sensing unify diffusion and quorum sensing? *Nature Reviews Microbiology* **5**, 230-239.
528 (doi:10.1038/nrmicro1600).

529 [37] Loomis, W.F. 2014 Cell signaling during development of dictyostelium. *Dev. Biol.* **391**, 1-16.
530 (doi:10.1016/j.ydbio.2014.04.001).

531 [38] Stingl, K., Altendorf, K. & Bakker, E.P. 2002 Acid survival of *Helicobacter pylori*: How does urease
532 activity trigger cytoplasmic pH homeostasis? *Trends Microbiol.* **10**, 70-74. (doi:10.1016/S0966-
533 842X(01)02287-9).

534 [39] Xue, C., Budrene, E.O. & Othmer, H.G. 2011 Radial and spiral stream formation in *proteus*
535 *mirabilis* colonies. *PLoS Comp. Biol.* **7**. (doi:10.1371/journal.pcbi.1002332).

536 [40] Yadav, V., Pavlick, R.A., Meckler, S.M. & Sen, A. 2014 Triggered detection and deposition:
537 Toward the repair of microcracks. *Chem. Mater.* **26**, 4647-4652. (doi:10.1021/cm5022323).

538 [41] Jagers, R.W. & Bon, S.A.F. 2017 Independent responsive behaviour and communication in
539 hydrogel objects. *Materials Horizons* **4**, 402-407. (doi:10.1039/c7mh00033b).

540 [42] Wrobel, M.M., Bánsági Jr, T., Scott, S.K., Taylor, A.F., Bounds, C.O., Carranzo, A. & Pojman, J.A.
541 2012 PH wave-front propagation in the urea-urease reaction. *Biophys. J.* **103**, 610-615.
542 (doi:10.1016/j.bpj.2012.06.020).

543 [43] Schuszter, G., Gehér-Herczegh, T., Szucs, Á., Tóth, Á. & Horváth, D. 2017 Determination of the
544 diffusion coefficient of hydrogen ion in hydrogels. *PCCP* **19**, 12136-12143. (doi:10.1039/c7cp00986k).

545 [44] Horváth, J., Szalai, I. & De Kepper, P. 2009 An experimental design method leading to chemical
546 turing patterns. *Science* **324**, 772-775. (doi:10.1126/science.1169973).

547 [45] Caplan, S.R., Naparstek, A. & Zabusky, N.J. 1973 Chemical oscillations in a membrane. *Nature*
548 **245**, 364-366. (doi:10.1038/245364a0).

549 [46] Míguez, D.G., Vanag, V.K. & Epstein, I.R. 2007 Fronts and pulses in an enzymatic reaction
550 catalyzed by glucose oxidase. *Proc. Natl. Acad. Sci. U.S.A.* **104**, 6992-6997.
551 (doi:10.1073/pnas.0611438104).

552 [47] Ghoshal, G., Muñozuri, A.P. & Pérez-Mercader, J. 2016 Emergence of a super-synchronized
553 mobbing state in a large population of coupled chemical oscillators. *Scientific Reports* **6**.
554 (doi:10.1038/srep19186).

555 [48] Szabo, E. 2015 Oregonator generalization as a minimal model of quorum sensing in Belousov-
556 Zhabotinsky reaction with catalyst confinement in large populations of particles. *RSC Advances* **5**,
557 99547-99554. (doi:10.1039/c5ra12841b).

558 [49] Semenov, S.N., Kraft, L.J., Ainla, A., Zhao, M., Baghbanzadeh, M., Campbell, V.E., Kang, K., Fox,
559 J.M. & Whitesides, G.M. 2016 Autocatalytic, bistable, oscillatory networks of biologically relevant
560 organic reactions. *Nature* **537**, 656-660. (doi:10.1038/nature19776).

561 [50] Bottero, I., Huck, J., Kosikova, T. & Philp, D. 2016 A Synthetic Replicator Drives a Propagating
562 Reaction-Diffusion Front. *J. Am. Chem. Soc.* **138**, 6723-6726. (doi:10.1021/jacs.6b03372).

563 [51] Semenov, S.N., Wong, A.S.Y., Van Der Made, R.M., Postma, S.G.J., Groen, J., Van Roekel, H.W.H.,
564 De Greef, T.F.A. & Huck, W.T.S. 2015 Rational design of functional and tunable oscillating enzymatic
565 networks. *Nature Chemistry* **7**, 160-165. (doi:10.1038/nchem.2142).

- 566 [52] Mukherjee, R., Cohen-Luria, R., Wagner, N. & Ashkenasy, G. 2015 A Bistable Switch in Dynamic
567 Thiopeptide Folding and Template-Directed Ligation. *Angewandte Chemie - International*
568 *Edition* **54**, 12452-12456. (doi:10.1002/anie.201503898).
- 569 [53] Gines, G., Zadorin, A.S., Galas, J.C., Fujii, T., Estevez-Torres, A. & Rondelez, Y. 2017 Microscopic
570 agents programmed by DNA circuits. *Nature Nanotechnology* **12**, 351-359.
571 (doi:10.1038/nnano.2016.299).
- 572 [54] Zenk, J., Scalise, D., Wang, K., Dorsey, P., Fern, J., Cruz, A. & Schulman, R. 2017 Stable DNA-
573 based reaction-diffusion patterns. *RSC Advances* **7**, 18032-18040. (doi:10.1039/c7ra00824d).
- 574 [55] Ashkenasy, G., Hermans, T.M., Otto, S. & Taylor, A.F. 2017 Systems chemistry. *Chem. Soc. Rev.*
575 **46**, 2543-2554. (doi:10.1039/c7cs00117g).

576